



1 **Organic aerosol in the summertime Southeastern United States: Components and**
2 **their link to volatility distribution, oxidation state and hygroscopicity**

3
4 Evangelia Kostenidou^{1,2}, Eleni Karnezi³, James R. Hite Jr⁴, Aikaterini Bougiatioti^{4,6}, Kate
5 Cerully^{5a}, Lu Xu^{5,b}, Nga L. Ng^{5,4}, Athanasios Nenes^{1,4,5,6*} and Spyros N. Pandis^{1,2,3*}

6
7 ¹Institute of Chemical Engineering Sciences, Foundation for Research and Technology,
8 Hellas, Patras, Greece

9 ²Department of Chemical Engineering, University of Patras, Patras, Greece

10 ³Department of Chemical Engineering, Carnegie Mellon University, Pittsburgh, USA

11 ⁴School of Earth and Atmospheric Sciences, Georgia Institute of Technology, Atlanta,
12 GA, USA

13 ⁵School of Chemical and Biomolecular Engineering, Georgia Institute of Technology,
14 Atlanta, GA, USA

15 ⁶Institute for Environmental Research and Sustainable Development, National
16 Observatory of Athens, Palea Penteli, Greece

17 ^anow at: TSI, Inc., Shoreview, MN, USA

18 ^bnow at: Division of Geological and Planetary Sciences, California Institute of
19 Technology, Pasadena, CA, USA

20
21 *correspondence to athanasios.nenes@gatech.edu, spyros@chemeng.upatras.gr

22
23 **Abstract**

24 The volatility distribution of the organic aerosol (OA) and its sources during the Southern
25 Oxidant and Aerosol Study (SOAS; Centerville, Alabama) was constrained using
26 measurements from an Aerodyne High-Resolution Time-of-Flight Aerosol Mass
27 Spectrometer (HR-ToF-AMS) and a thermodenuder. Positive Matrix Factorization (PMF)
28 analysis was applied on both the ambient and thermodenuded high resolution mass
29 spectra, leading to four factors: more oxidized oxygenated OA (MO-OOA), less oxidized
30 oxygenated OA (LO-OOA), an isoprene epoxydiols (IEPOX) related factor (Isoprene-
31 OA) and biomass burning OA (BBOA). BBOA had the highest mass fraction remaining



32 (MFR) at 100°C, followed by the isoprene-OA, and the LO-OOA. Surprisingly the MO-
33 OOA evaporated the most in the TD. The estimated effective vaporization enthalpies
34 assuming an evaporation coefficient equal to unity were 58 ± 13 kJ mol⁻¹ for the LO-OOA,
35 89 ± 10 kJ mol⁻¹ for the MO-OOA, 55 ± 11 kJ mol⁻¹ for the BBOA, and 63 ± 15 kJ mol⁻¹ for
36 the Isoprene-OA. The estimated volatility distribution of all factors covered a wide range
37 including both semi-volatile and low-volatility components. BBOA had the lowest
38 average volatility of all factors, even though it had the lowest O:C ratio among all factors.
39 LO-OOA was the more volatile factor and its high MFR was due according to the model
40 to its low enthalpy of vaporization. The Isoprene-OA factor had intermediate volatility,
41 quite higher than suggested by a few other studies. The analysis suggests that deducing
42 the volatility of a factor only from its MFR could lead to erroneous conclusions. The
43 oxygen content of the factors can be combined with their estimated volatility and
44 hygroscopicity to provide a better view of their physical properties.

45

46 1. Introduction

47 Population exposure to atmospheric particulate matter (PM) increases premature
48 mortality from cardiovascular and respiratory diseases (Pope et al., 2002; IARC, 2013;
49 Cohen et al., 2017). The same particles also modulate the planetary radiative balance and
50 hydrological cycle (IPCC, 2013; NASEM, 2016; Seinfeld et al., 2016). Organic aerosol
51 (OA) constitutes a significant part of submicron aerosol mass (Zhang et al., 2007) and it
52 is characterized by daunting chemical complexity (Kanakidou et al., 2005; Hallquist et al.,
53 2009). OA is directly emitted from anthropogenic and natural sources, but it is also
54 produced by condensation of products formed during the oxidation of gas-phase organic
55 compounds with O₃, NO₃ and OH radicals (secondary organic aerosol, SOA; Kanakidou
56 et al., 2005). OA formation can be further promoted by the interactions of anthropogenic
57 and biogenic compounds; in the southeastern United States, anthropogenic sulfate
58 enhances OA formation through rapid reactive uptake of IEPOX to particles and aqueous
59 phase reactions (Xu et al., 2015a; Xu et al., 2016a; Budisulistiorini et al., 2017).

60 Several approaches have been developed to unravel the sources and the degree of
61 atmospheric processing of aerosol sampled by the AMS. These include custom principal
62 component analysis (Zhang et al., 2005), multiple component analysis (Zhang et al.,



63 2007), PMF (Paatero and Tapper 1994; Lanz et al., 2007) and the multilinear engine
64 (ME-2) (Lanz et al., 2008; Canonaco et al., 2013). Applying the above source
65 apportionment techniques on AMS mass spectra, information about the aerosol sources
66 and the degree of the atmospheric processing can be derived. Important primary
67 components include hydrocarbon-like OA (HOA) (Zhang et al., 2005) and biomass
68 burning OA (BBOA) (Aiken et al., 2009). The most abundant and ubiquitous OA
69 component is the oxygenated OA (OOA), which often consists of a more oxygenated
70 (MO-OOA) and a less oxygenated OA (LO-OOA) factor (Lanz et al., 2007). In the
71 southeastern (SE) United States, MO-OOA and LO-OOA are dominant factors,
72 comprising 47-79% of the total OA (Xu et al., 2015b). Factors related to biogenic
73 secondary OA have been identified in urban, suburban and remote areas (Budisulistiorini
74 et al., 2013; Chen et al., 2015; Kostenidou et al., 2015). In the SE United States, an
75 Isoprene-OA factor linked to IEPOX uptake is present during warm periods, contributing
76 up to 36% of the total OA in the summertime (Xu et al., 2015b).

77 Central to understanding the atmospheric impacts of OA is constraining its
78 volatility and hygroscopicity (Kanakidou et al., 2005). Volatility measurements are mostly
79 carried out using heated laminar flow reactors, known as thermodenuders (TD)
80 (Burtscher et al., 2001; An et al., 2007) or isothermal dilution (Grieshop et al., 2009). In
81 these systems, changes in OA mass concentration are related to the OA evaporation rate
82 and its volatility can be estimated. The comparison of aerosol evaporation measurements
83 across studies and conditions with TD or isothermal dilution chambers is not
84 straightforward. The established proxy for volatility is the “mass fraction remaining
85 (MFR)”, i.e., the mass of the aerosol remaining after a volatility measurement (Huffman
86 2009; Cerully et al., 2015; Xu et al., 2016b). MFR has often been used as a relative
87 measure of volatility, as it is assumed that the volatility of particulate matter increases as
88 MFR decreases for particles and TD conditions that are otherwise identical. Although
89 clearly linked to volatility, the MFR depends on the enthalpy of vaporization (ΔH_{vap}), the
90 aerosol concentration, the heating section residence time, the particle size distribution,
91 and potential particle-to-gas mass transfer resistances. All these parameters therefore
92 complicate the linking of the measured MFR to the volatility. An additional complication
93 is that organic aerosol mixtures are characterized by a distribution of volatilities. A



94 number of studies have attempted to estimate this volatility distribution with appropriate
95 TD models (Cappa and Jimenez, 2010; Lee et al., 2010; Paciga et al., 2016; Saha and
96 Grieshop 2016; Louvaris et al., 2017; Saha et al., 2017).

97 Three studies have reported volatility distributions of the isoprene (or IEPOX)
98 SOA and the total OA for the southeastern United States. Lopez-Hilfiker et al. (2016)
99 suggested that the IEPOX SOA had a very low saturation concentration with $C^*=10^{-4}$ μg
100 m^{-3} , based on the FIGAERO-CIMS signals of $\text{C}_5\text{H}_{12}\text{O}_4$ and $\text{C}_5\text{H}_{10}\text{O}_3$. They assumed that
101 these signals correspond to 2-methyltetrols and 3-MeTHF-3,4-diols and/or C5 alkene
102 triols, which are tracers for isoprene SOA. Using the total FIGAERO-CIMS signal
103 ($\text{C}_x\text{H}_y\text{O}_z\text{N}_{0-1}$) the same authors estimated an extremely low total OA average volatility of
104 $C^*=3.7 \times 10^{-7}$ μg m^{-3} for the OA with ELVOCs representing 99% of the total. This is the
105 lowest reported volatility for ambient OA in the literature. Hu et al. (2016) estimated an
106 average volatility of $C^*=5.2 \times 10^{-5}$ μg m^{-3} for the IEPOX SOA. Their results were based on
107 the MFR of the IEPOX SOA (calculated by PMF) using ambient and thermodenuded
108 AMS measurements. The volatility distribution of IEPOX SOA was estimated applying
109 the technique of Faulhaber et al. (2009). The corresponding total OA volatility
110 distribution covered the range from $C^*=10^{-9}$ to 1 μg m^{-3} . Saha et al. (2017) used an
111 Aerosol Chemical Speciation Monitor (ACSM) and a thermodenuder to estimate an
112 average total OA volatility of $C^*=0.21$ μg m^{-3} and a vaporization enthalpy of 100 kJ mol^{-1} .

113 The two-dimensional volatility basis set (2D-VBS) framework, describing the
114 OA concentration as a function of its oxygen content and volatility is a promising
115 approach to describe the partitioning and chemical evolution of the thousands of
116 compounds present in OA (Donahue et al., 2012). If expanded to include hygroscopicity,
117 the framework can be strengthened considerably. Several studies have attempted to link
118 hygroscopicity and volatility (Kuwata et al., 2007; Asa-Awuku et al., 2009; Frosh et al.,
119 2013) or hygroscopicity and oxidation state (Masoli et al., 2010; Chang et al., 2010;
120 Lathem et al., 2013; Thalman et al., 2017), however only a few focus on all the properties
121 combined (Jimenez et al., 2009; Tritscher et al., 2011; Cerully et al., 2015). Jimenez et al.
122 (2009) combined data from various studies and suggested that hygroscopicity and
123 oxidation state increase as volatility decreases. The generality of this finding has been
124 questioned by subsequent studies (Meyer et al., 2009; Tritscher et al., 2011; Lathem et al.,



125 2013). Recently, Nakao (2017) proposed a theoretical framework, in which the
126 hygroscopicity is explicitly related to oxidation state and volatility. With this approach,
127 each OA “source” can have a unique set of volatility and hygroscopicity parameters that
128 evolve with atmospheric oxidative aging – along a path that requires further constraints
129 from chemistry.

130 In this study we build upon the work of Xu et al. (2015a) and Cerully et al. (2015)
131 and attempt to constrain the volatility distributions and effective vaporization enthalpy of
132 each PMF factor of OA sampled during the SOAS field campaign at Centreville,
133 Alabama. We then proceed to associate the hygroscopicity parameters estimated by
134 Cerully et al. (2015) with the volatility distributions and test their consistency with the
135 Nakao (2017) theoretical framework.

136

137 2. Experimental

138 2.1 Measurement site and campaign

139 The measurements were performed in Centreville, Alabama, (32°54'11.81"N,
140 87°14'59"W). The station was located in an area significantly influenced by biogenic
141 emissions (Liao et al., 2007; Spracklen et al., 2011). Anthropogenic emissions also affect
142 the site. The measurements were conducted during the Southern Oxidant and Aerosol
143 Study (SOAS), which was part of the Southern Atmosphere Study (SAS;
144 <http://www.eol.ucar.edu/projects/sas>) from June 1 to July 15 2013. A summary of
145 important findings can be found in Carleton et al. (2017), while additional results relevant
146 for our study can be found in Xu et al. (2015a), Cerully et al. (2015), Guo et al. (2015)
147 and Saha et al. (2017).

148

149 2.2 Instrumentation

150 The aim of the specific measurements was to characterize both the ambient and
151 the water soluble fraction of the non-thermally and thermally-denuded PM₁. For the
152 vaporization a thermodenuder, TD, (Cerully et al., 2014) was used. A particle-into-liquid
153 sampler (PILS) (Weber et al., 2001) was used to collect the water soluble aerosol
154 components and then the solution was nebulized. The aerosol passed every 12 or 15 min
155 through four lines: ambient bypass, ambient TD, PILS bypass and PILS TD. In this work



156 we used the ambient denuded measurements only. Details about the experimental set up
157 can be found in Cerully et al. (2015).

158 The sampling instrumentation included an Aerodyne HR-AMS, a Scanning
159 Mobility Particle Sizer (SMPS, Classifier model 3080, DMA model 3081, CPC model
160 3022A, TSI), a Cloud Condensation Nuclei counter (CCNc, Droplet Measurement
161 Technologies). The TD used in this campaign has been characterized by Cerully et al.
162 (2014). Briefly, the TD consisted of a heating and a cooling section. The first part was a
163 stainless steel tube 30 with in length and 0.68 in inner diameter. The cooling section was
164 removed during this campaign, as the re-condensation of the vapors is minimal when the
165 ambient mass concentration is low, which was the case for this campaign (Cappa et al.,
166 2010; Saleh et al., 2011; Cerully et al., 2014). The temperature in the TD was 60, 80 and
167 100°C. The total flow rate passing through the TD was 1.5 L min⁻¹ and so the average TD
168 residence time was approximately 7 s.

169

170 **3. Data Analysis**

171 **3.1 PMF and elemental ratios**

172 PMF (Lanz et al., 2007) was applied to both ambient bypass and TD HR organic
173 mass spectra according to the procedure of Ulbrich et al. (2009). Details about the PMF
174 solution are provided in the SI (Figures S1 and S2). The O:C and H:C elemental ratios
175 were estimated using the approach of Canagaratna et al. (2015). Xu et al. (2015a) also
176 used the Canagaratna et al. (2015) O:C approach, however Cerully et al. (2015) applied
177 the older algorithm of Aiken et al. (2008). For any comparisons between this work and
178 previous studies we converted the old O:C to the new O:C ratios using the corresponding
179 f_{44} fraction according to the equation: $O:C = 0.079 + 4.31 f_{44}$ (Canagaratna et al., 2015).

180

181 **3.2 Collection efficiency (CE)**

182 Xu et al. (2015a) estimated the AMS CE using the composition-dependent
183 approach of Middlebrook et al. (2012). The average bypass CE was estimated to be
184 0.65 ± 0.12 , while the average TD CE was slightly higher 0.7 ± 0.11 . The difference was
185 statistically significant with a p value less than 0.0001. These estimates can be more



186 uncertain than their variability suggests, due to their sensitivity to aerosol ammonium and
187 neutralization. The sensitivity of our results is discussed in Section 5.3.

188

189 **3.3 TD losses**

190 The thermodenuded OA was corrected for particle losses due to sedimentation,
191 diffusion and thermophoresis inside the thermodenuder. More details about the
192 thermodenuder characterization are provided by Cerully et al. (2014).

193

194 **3.4 MFR**

195 For the MFR calculations only data with ambient OA concentration higher than
196 $0.2 \mu\text{g m}^{-3}$ were used in order to avoid extreme variations of the MFR. For such low
197 concentrations the corresponding TD concentrations can be very low introducing
198 significant error in the MFR calculation. The fractions of the data for each factor above
199 the threshold of $0.2 \mu\text{g m}^{-3}$ are given in Table 1. For the total OA, MO-OOA and LO-
200 OOA this fraction was above 92% but for the Isoprene-OA and BBOA was lower (76%
201 and 42% respectively). The four (or five) consecutive ambient and TD measurements
202 during each hour were averaged. The variability of the four (or five) averaged values was
203 4-16%.

204

205 **3.5 Volatility distribution estimation**

206 The dynamic mass transfer model of Riipinen et al. (2010) was used to estimate the OA
207 volatility distributions. The model simulates the particle evaporation inside the
208 thermodenuder solving the corresponding system of differential equations describing the
209 mass transfer between the particle and gas phases:

$$210 \quad \frac{dm_p}{dt} = -\sum_{i=1}^n I_i \quad (1)$$

$$211 \quad \frac{dC_i}{dt} = I_i N_{tot} \quad (2)$$

212 where m_p is the organic particle mass, C_i is the gas-phase concentration of compound i ,
213 N_{tot} is the total number concentration of the particles, n is the number of the assumed



214 organic aerosol components, and I_i the mass flux of the compound i given by the Vesala
215 et al. (1997) equation:

$$216 \quad I_i = \frac{2\pi d_p p M_i D_i \beta_{mi}}{RT_{TD}} \ln \left[\frac{1 - \frac{p_i}{p}}{1 - \frac{p_i^0}{p}} \right] \quad (3)$$

217 where d_p is the particle diameter, R the molar gas constant, M_i and D_i the molar mass and
218 the diffusion coefficient of compound i at temperature T_{TD} . The diffusion coefficient (D_i)
219 depends on the temperature and is calculated according to Chen and Othmer (1962) and
220 β_{mi} is the correction factor given by Fuchs and Sutugin (1970). p is the total gas pressure,
221 while p_i and p_i^0 are the partial vapor pressures of the compound i at the particle surface
222 and far away from the particle respectively. p_i^0 is given by:

$$223 \quad p_i^0 = x_i \gamma_i p_{sat,i} \exp\left(\frac{4M_i \sigma}{RT_p \rho d_p}\right) = x_{mi} \frac{C_i^* RT_{TD}}{M_i} \exp\left(\frac{4M_i \sigma}{RT_p \rho d_p}\right) \quad (4)$$

224 where x_i is the mole fraction of i , γ_i the activity coefficient of i in the particle, $p_{sat,i}$ the
225 pure component vapor pressure of i over a flat surface, T_p the particle temperature (we
226 assume that $T_p = T_{TD}$), x_{mi} the mass fraction of i in the particle, ρ the particle density and σ
227 the particle surface tension. C_i^* is the effective saturation concentration of i at 298 K.

228 The change of the vapor pressure with temperature is calculated by the Clausius-
229 Clapeyron equation:

$$230 \quad C_i^*(T_{TD}) = C_i^*(298\text{ K}) \exp\left[\frac{\Delta H_{vap,i}}{R} \left(\frac{1}{298} - \frac{1}{T_{TD}}\right)\right] \frac{298}{T_{TD}} \quad (5)$$

231 where ΔH_{vap} is the vaporization enthalpy of component i .

232 The model inputs include the loss corrected MFRs, the thermodenuder
233 temperature and residence time, the bypass average particle size and the OA
234 concentration. The output of the model is the OA volatility distribution in terms of
235 effective saturation concentrations (C^*) at 298 K, in combination with its effective
236 vaporization enthalpy (ΔH_{vap}) and the mass accommodation (evaporation) coefficient
237 (a_m). We fit the measured thermograms using a consecutive 3-bin C^* distribution, with
238 varying mass fraction in each bin. The bins corresponded to saturation concentrations of
239 0.1, 1, and 10 $\mu\text{g m}^{-3}$ at 298K. The enthalpy of vaporization (ΔH_{vap}) was also estimated,



240 while the accommodation coefficient was assumed to be equal to unity. The best
241 (optimum) solutions and the corresponding uncertainties are calculated using the
242 approach of Karnezi et al. (2014). For each solution the average mass fraction in each bin
243 and its corresponding standard deviation, was estimated using the top 2% of the mass
244 fraction combinations with the lowest error. In this study for the comparison between
245 volatilities we will use the average volatility based on mass fraction weighted $\log_{10}C^*$.

246

247 3.6 Hygroscopicity

248 Details about the hygroscopicity analysis of the corresponding data can be found
249 in Cerully et al. (2015). Using a CCNc Cerully et al. (2015) estimated the hygroscopicity
250 parameter κ of the total and water soluble ambient and thermodenuded PM_{10} OA. The
251 same authors performed linear regression of the ambient water soluble κ_{org} with the PMF
252 factors of the ambient water soluble OA. During the periods of the water solubility
253 measurements the BBOA concentration was too low to allow the separation of the factor,
254 so its hygroscopicity was not determined. The PMF results of the ambient total and the
255 ambient water soluble data were practically the same.

256

257 4. Results and Discussion

258 4.1 Volatility of organic aerosol

259 The average OA mass concentration was $5 \mu\text{g m}^{-3}$. The loss-corrected OA MFR is
260 depicted in Figure 1a. Half of the total OA evaporated at 100°C ($T_{50}=100^\circ\text{C}$). The
261 estimated volatility distribution (Figure 1b) indicates that 46% of the organic aerosol was
262 semivolatile organic compounds (SVOCs) (compounds with $1 \leq C^* \leq 100 \mu\text{g m}^{-3}$) and
263 54% was low volatility organic compounds (LVOCs) ($0.001 \leq C^* \leq 0.1 \mu\text{g m}^{-3}$). Part of
264 the material assigned to the $0.1 \mu\text{g m}^{-3}$ bin has volatility less than this value. The fact that
265 there were no measurements above 100°C does not allow us to constrain further the
266 contributions of the LVOCs and ELVOCs. The average volatility based on mass fraction
267 weighted $\log_{10}C^*$ values was $C^*=0.55\pm 0.29 \mu\text{g m}^{-3}$. Please note that this value is useful
268 only for comparisons of volatility distributions in the same VBS volatility range. The
269 mass fraction of each volatility bin is provided in Table S1. The effective vaporization
270 enthalpy of the total OA was $86\pm 9 \text{ kJ mol}^{-1}$.



271

272 **4.2 Volatility of OA components**

273 The PMF analysis using both the ambient and TD measurements suggested four
274 factors. The OA consisted of 43% more oxidized OOA (MO-OOA), 29% less oxidized
275 OOA (LO-OOA), 19% Isoprene-OA and 9% biomass burning OA (BBOA). The same
276 four factors and OA composition were obtained by Xu et al. (2015a) using only the
277 ambient AMS HR mass spectra (Table 2). Details about their characteristics, correlation
278 with external tracers and justification of their names are provided by Xu et al. (2015a).
279 The ambient OA factor time series were practically the same in the two analyses with
280 $R^2 > 0.93$, the mass spectra were also similar with angle θ equal to 3-4 degrees for LO-
281 OOA, MO-OOA and Isoprene-OA and 12 degrees for the BBOA factor (Figure S3).
282 Thus, our PMF results are robust and quite consistent with the previous analysis.

283 The loss-corrected MFRs of the four factors are depicted in Figure 2. BBOA
284 evaporated less, as its MFR was close to unity at all temperatures. The BBOA factor was
285 quite oxygenated with an O:C of 0.58 compared to previous studies (e.g., Crippa et al.,
286 2013; Florou et al., 2017). The corresponding BBOA could be chemically aged or PMF
287 may be mixing the BBOA with aged background OA. Even though BBOA and Isoprene-
288 OA had similar O:C ratios (0.58 and 0.59 correspondingly), the Isoprene-OA MFR was
289 lower. Surprisingly the MFR of MO-OOA was lower than that of LO-OOA, even though
290 MO-OOA had a higher O:C ratio (0.99) than LO-OOA (0.63). Relying only on MFR
291 one would reach the conclusion that MO-OOA was more volatile than LO-OOA.

292 The predicted thermograms for each factor are also depicted in Figure 2 and the
293 resulting volatility distributions are shown in Figures 3a-3d. Figures 3e and 3f show the
294 comparison of the volatility compositions and the vaporization enthalpies between the
295 four OA factors. The mass fractions of each volatility bin (in the aerosol phase), average
296 volatility (C^*) and the vaporization enthalpy of each factor are given in Table S1.

297 The average LO-OOA mass concentration was $1.66 \mu\text{g m}^{-3}$ and this factor based
298 on the model was composed of 73% SVOCs and 27% LVOCs. Its average volatility was
299 $C^* = 1.88 \pm 0.32 \mu\text{g m}^{-3}$ and its effective vaporization enthalpy $58 \pm 13 \text{ kJ mol}^{-1}$. The average
300 MO-OOA mass concentration was $1.96 \mu\text{g m}^{-3}$. According to its volatility distribution
301 56% of the MO-OOA was SVOCs and 44% was LVOCs. Its effective vaporization



302 enthalpy was 89 ± 10 kJ mol⁻¹ and its average volatility 0.95 ± 0.31 μg m⁻³. According to
303 least to the model the MO-OOA was less volatile on average than the LO-OOA even if it
304 evaporated more in the TD. This counterintuitive behavior is explained by the TD model
305 by the higher effective vaporization enthalpy of the MO-OOA, probably due to the
306 contribution of dicarboxylic and tricarboxylic acids which have vaporization enthalpies
307 higher than 100 kJ mol⁻¹ (e.g., Saleh et al., 2008; 2010; Kostenidou et al., submitted) Our
308 results suggest that deducing the volatility of a component using only its MFR or its O:C
309 ratio may lead to incorrect conclusions This finding is also supported by Xu et al. (2016b),
310 where they suggest that different O:C distributions could result in the same bulk O:C but
311 different volatility distributions, which may lead to particles with the same O:C but
312 different MFR.

313 BBOA was the less abundant factor with average mass concentration equal to 0.5
314 μg m⁻³. According to the TD model, 53% of the BBOA consisted of SVOCs and the other
315 47% was LVOCs. Its average volatility was $C^* = 0.59 \pm 0.22$ μg m⁻³ and its effective
316 vaporization enthalpy was 55 ± 11 kJ mol⁻¹. Finally, the average Isoprene-OA mass
317 concentration was 0.9 ± 0.5 μg m⁻³ and composed of 59% SVOCs and 41% LVOCs. Its
318 estimated average volatility was $C^* = 1.05 \pm 0.30$ μg m⁻³ and its vaporization enthalpy
319 63 ± 15 kJ mol⁻¹.

320 These results suggest that all factors contained components with a wide range of
321 volatilities. Based on their average volatility BBOA was the least volatile, followed by
322 MO-OOA, Isoprene-OA and finally LO-OOA was the more volatile OA component. The
323 availability of measurements at only three temperatures introduces uncertainty in the
324 above results. A detailed sensitivity analysis is presented in Section 5.

325

326 5. Sensitivity analysis

327 5.1 Effective enthalpy of vaporization (ΔH_{vap})

328 We estimated the volatility distributions for three fixed vaporization enthalpies: 50, 80
329 and 100 kJ mol⁻¹ for all factors (Table S2). While the corresponding thermograms do not
330 reproduce as well the corresponding measurements, it is instructive to examine the
331 corresponding volatility distributions taking into account this time the measurement
332 uncertainties.



333 The 80 and 100 kJ mol⁻¹ values lead to thermograms for MO-OOA consistent with
334 the measurements given the uncertainty of the latter (Figure A1, Appendix). The resulting
335 MO-OOA volatility distributions (Figure A2, Appendix) are within the uncertainty range
336 of the distributions shown in Figure 3. The LVOC content of the factor varies from 35%
337 to 60% as the ΔH_{vap} varies from 80 to 100 kJ mol⁻¹. The optimum (base case) solution
338 suggested a 44% LVOC content.

339 The situation is a little more complex for LO-OOA due to the higher variability of
340 the corresponding MFR measurements. All three ΔH_{vap} values lead to solutions that are
341 consistent with the observations within experimental uncertainty. This results in a wide
342 range of volatility distributions with the LVOC content varying from 25% to 90% (Figure
343 A2). The best (base case) solution suggested 27% LVOCs, so the sensitivity analysis
344 suggests that the LO-OOA may have been significantly less volatile.

345 Only the 50 and 80 kJ mol⁻¹ values lead to acceptable thermograms for the
346 Isoprene OA (Figure A1). The LVOCs are predicted to contribute to the factor from 35 to
347 75% (Figure A2) as the assumed ΔH_{vap} varies from 50 to 80 kJ mol⁻¹. The optimum (base
348 case) solution corresponded to 41% LVOCs.

349 Finally, for the BBOA as the ΔH_{vap} varies from 50 to 80 kJ mol⁻¹ (the 100 kJ
350 mol⁻¹ value does not lead to acceptable solutions) the LVOC content increases from 65 to
351 87% (Figure A2), values that are higher than the estimated 47% LVOCs in the optimum
352 (base case) solution.

353

354 5.2 Accommodation coefficient

355 It has been assumed in the analysis so far that there were no resistances to the
356 evaporation of the OA in the TD and that the accommodation coefficient, a_m , was equal
357 to one. We performed two sensitivity tests using accommodation coefficients of one and
358 two orders of magnitude lower (0.1, 0.01). The volatility distributions, the average
359 volatility C^* and the vaporization enthalpy of each factor are given in Table S1. The
360 corresponding MFRs are illustrated in Figure A3 and the volatility distributions in Figure
361 A4.

362 A value of a_m equal to 0.01 is inconsistent with the measured thermograms of
363 MO-OOA, Isoprene-OA and total OA (Figure A3). For LO-OOA and BBOA the



364 predicted thermograms are within the experimental error of the measured values and the
365 resulting volatility distributions are quite close to those of the base case. For example, for
366 LO-OOA the LVOC content is 40% (Figure A4) compared to 27% in the optimum
367 solution. This rather surprising insensitivity of the volatility distribution is that the model
368 balances the effects of the lower a_m with an increase of the predicted ΔH_{vap} . In the case of
369 the LO-OOA the estimated enthalpy of vaporization increases to 121 kJ mol^{-1} .

370 The intermediate value of $a_m=0.1$ leads to predicted MFR values within the
371 experimental error for LO-OOA, Isoprene-OA and BBOA, but not for MO-OOA or total
372 OA (Figure A3). For the acceptable cases the average volatility of the OA components
373 decreases by a factor of 2-3 and the effective ΔH_{vap} increases by 30-40 kJ mol^{-1} . The
374 LVOC content of LO-OOA increases from 27% to 52%, while the increase of the
375 Isoprene-OA and BBOA LVOCs is small (from 41 to 47% and from 60 to 64%)
376 respectively (Figure A4).

377 For the MO-OOA and the total OA only the $a_m=1$ simulations provided
378 acceptable results.

379 The above analysis suggests that the estimated volatility distributions have a
380 surprisingly low sensitivity to the assumed evaporation coefficient, but the ΔH_{vap} is quite
381 sensitive to this value. This result is quite different from other studies (e.g., Lee et al.,
382 2010; Cappa and Jimenez 2010; Riipinen et al., 2010) and is due to the limited
383 temperature range of the measurements in the present work.

384

385 **5.3 TD collection efficiency**

386 In this case we repeated the calculations assuming a lower AMS CE for the
387 aerosol that passed through the TD. Assuming a 10% lower CE in the TD, the volatility
388 distribution of MO-OOA and Isoprene-OA changed by less than 10% (Table S1).
389 However, the volatility distribution of LO-OOA and BBOA shifted towards lower values
390 with the average volatility decreasing by around a factor of 2. The reasons for this
391 behavior could be the high LO-OOA MFR uncertainty and the low mass concentration of
392 the BBOA. The corresponding thermograms and volatility distribution are shown in
393 Figures S4 and S5.

394



395 **6. Comparisons with other studies**

396 **MO-OOA and LO-OOA:** The volatility distributions of the MO-OOA and LO-OOA
397 were similar to those of the aged aerosol in Finokalia (FAME-08) (Lee et al., 2010) in
398 which the SVOCs accounted for 60% and LVOCs for 40% of the OA using an $a_m=0.05$
399 and $\Delta H_{\text{vap}}=80 \text{ kJ mol}^{-1}$ (Figure S7). The SOAS LO-OOA appears to be a little more
400 volatile than the summertime SV-OOA in Paris (Paciga et al., 2016) and Mexico City
401 (Cappa et al., 2010), while the MO-OOA is a lot more volatile than the LV-OOA in these
402 locations. These summertime OOA components in SOAS were more volatile compared
403 to the wintertime OOA in Paris and Athens (Louvaris et al., 2017), which had a lower
404 SVOC content (45% for Paris and 31% in Athens).

405

406 **BBOA:** Figure S6b illustrates the volatility comparisons between the BBOA factor and
407 the BBOA factors from Mexico City, Paris (winter) and Athens (winter). The estimated
408 SVOC content of all four BBOA factors was surprisingly similar around 50% with the
409 Mexico City BBOA having the higher fraction (70%). The differences in LVOCs and
410 ELVOCs are at least partially due to the temperature ranges used in the corresponding
411 measurements. The corresponding O:C ratios of the factors were quite different, 0.58 for
412 SOAS, 0.4 for Mexico City, 0.29 for Paris, and 0.23 for Athens (all estimated using the
413 Canagaratha et al. (2015) approach). Part of the reason of the discrepancy may be hidden
414 in the least volatile components of BBOA that were not examined in the present study.

415

416 **Isoprene-OA:** Lopez-Hilfiker et al. (2016) suggested that the IEPOX SOA had much
417 lower saturation concentration, $C^*=10^{-4} \mu\text{g m}^{-3}$, compared to the volatility of the
418 Isoprene-OA estimated here. Potential reasons for the discrepancy may include the fact
419 that their conclusion was based on major components of IEPOX SOA and not all the
420 products, the fact that Isoprene-OA factor may not be entirely composed of IEPOX,
421 potential interactions of these components with the substrate used in FIGAERO-CIMS,
422 the role of the vaporization enthalpy in the thermal behavior of these compounds, etc.
423 As a consistency test, we used the volatility distribution of Lopez-Hilfiker et al. (2016) as
424 input to the code of Riipinen et al. (2010) varying the enthalpy of vaporization. The best
425 result was obtained for an abnormally high value of $\Delta H_{\text{vap}}=208 \text{ kJ mol}^{-1}$ and even then the



426 model underestimates the observed evaporation of Isoprene-OA (Figure S7). Using more
427 reasonable values of ΔH_{vap} for such compounds the discrepancies between our
428 measurements and the predictions are even larger, suggesting that the Lopez-Hilfiker et al.
429 (2016) volatility estimates are not consistent with our results and appear not to represent
430 the full volatility range of Isoprene-OA.

431 A similar discrepancy exists with the low estimated volatility for the IEPOX SOA
432 by Hu et al. (2016) which is even lower than that of Lopez-Hilfiker et al. (2016) (Figure
433 S6c). One reason for the discrepancy is that their estimate was based on the empirical
434 method of Faulhaber et al. (2009) which has been calibrated using the TD behavior of 5
435 known compounds and neglecting potential differences in ΔH_{vap} .

436 These discrepancies clearly show that there is need for additional investigation of
437 the volatility of the various components of the isoprene SOA in the atmosphere.

438

439 **Total OA:** Figure S6d compares the total OA volatility estimated in this study to those of
440 Lopez-Hilfiker et al. (2016), Hu et al. (2016), and Saha et al. (2017) for the same location
441 (Centreville) and period. To facilitate the comparison, given that different temperature
442 ranges were used in the above studies, the $C^*=0.1 \mu\text{g m}^{-3}$ bin is used to represent
443 compounds of even lower volatility than this value. Our results are quite consistent with
444 those of Saha et al. (2017) especially considering the differences in both the TD design
445 and modeling of the results. On the other hand, the Hu et al. (2016) and Lopez-Hilfiker et
446 al. (2016) results suggest an OA with much lower volatility that is inconsistent with our
447 TD measurements.

448

449 7. Link to the 2D-VBS framework

450 Figure 4 shows the location of our factors in the 2D-VBS framework of Donahue
451 et al. (2012). The PMF sources locations in the 2D-VBS were estimated using the
452 elemental ratios derived by the method of Aiken et al. (2008) for consistency with the
453 original figure. The O:C of the MO-OOA, LO-OOA, Isoprene-OA and BBOA factors
454 was 0.8, 0.46, 0.44 and 0.46 correspondingly. The MO-OOA factor is in the proposed
455 LV-OOA area but it includes a SVOC component that does not exist in the original 2D-
456 VBS. The LO-OOA factor is quite consistent with the proposed SV-OOA area. The



457 Isoprene-OA is also located in the SV-OOA area based on our results. Finally, the BBOA
458 factor has the expected volatility range, but is in the upper border of the 2D-VBS BBOA
459 area due to its high oxidation state observed during SOAS.

460

461 **8. Linking the hygroscopicity of OA components to their O:C ratio and volatility**

462 Cerrully et al. (2015) estimated the hygroscopicity κ parameter for each factor for
463 the SOAS campaign for supersaturation $s=0.4\%$ using PMF analysis on the PILS aerosol.
464 The resulting values were: $\kappa_{\text{MO-OOA}}=0.16\pm 0.02$, $\kappa_{\text{LO-OOA}}=0.08\pm 0.02$ and $\kappa_{\text{Isoprene-OA}}=$
465 0.20 ± 0.02 . During the periods of the PILS measurements the BBOA contribution was
466 very low and PMF could not resolve this factor. The Isoprene-OA factor had a higher κ
467 than MO-OOA, but its O:C ratio was lower (0.62) than MO-OOA (1.02). This contradicts
468 Jimenez et al. (2009) which proposed that the hygroscopicity increases linearly as the
469 O:C ratio increases and the recent study of Thalman et al. (2017) which suggested that for
470 OOA factors the relationship between the hygroscopicity and the O:C is linear.

471 A recent study by Nakao (2017) proposed a theoretical description for the linkage
472 between the O:C ratio, volatility and hygroscopicity. Figure S8 illustrates the
473 experimental saturation concentrations and κ parameters for known compounds found in
474 the literature (Table S3 and S4) together with the Nakao (2017) estimations. The isolines
475 in this figure represent the intrinsic κ which corresponds to the upper limit of κ assuming
476 that the organic species are entirely soluble. The location of the selected known
477 compounds was generally in agreement with the suggested by Nakao (2017) intrinsic κ
478 isolines for κ higher than 0.1. For κ lower than 0.1 the experimental values were
479 underestimated compared to the theoretical κ . This discrepancy could be due to the fact
480 that the compounds in the area with κ above 0.1 are more water soluble than those in the
481 area with κ below 0.1. For example, the solubility of malonic acid is 1161 g L^{-1} (Saxena
482 and Hildemann 1996), while the water solubility of suberic acid is 2.46 g L^{-1} (Bretti et al.,
483 2006).

484 Xu et al. (2017) calculated the water solubility of the MO-OOA, LO-OOA and
485 Isoprene-OA in Centreville during the SOAS campaign and found it 100%, 47% and 83%
486 correspondingly. Thus, the intrinsic κ of MO-OOA, LO-OOA and Isoprene-OA is
487 correspondingly 0.16 ± 0.02 , 0.17 ± 0.04 and 0.24 ± 0.03 . Figure 5 shows the intrinsic κ



488 values of our factors in the 2D-VBS and the Nakao (2017) frameworks. The MO-OOA
489 and LO-OOA values are close to the Nakao (2017) proposed intrinsic κ isolines.
490 However, the Isoprene-OA experimental intrinsic κ (0.24) is higher than the theoretical
491 (0.13). One reason for this disagreement could be the O:C estimate by the AMS.
492 Canagaratna et al. (2015) measured the O:C ratio of a racemic mixture of δ -Isoprene
493 epoxydiols ($C_5H_{10}O_3$) and found it around 0.4, which is 1.5 times lower than the
494 theoretical (0.6). If the Isoprene-OA factor behaves similarly to the racemic mixture, its
495 O:C may in fact be as high as 0.9, corresponding to a higher theoretical (Nakao 2017)
496 intrinsic $\kappa=0.19$, which is closer to the experimental value (0.24). Although our results
497 cannot be fully explained by the theoretical framework of (Nakao 2017), they denote that
498 the relationship between hygroscopicity, volatility and O:C ratio is rather complicated.
499 The model of Nakao (2017) is based on numerous assumptions that may not always be
500 valid and which could introduce errors in the κ isolines estimation. Recently, Rastak et al.
501 (2017) concluded that the hygroscopicity should be described using more than a single
502 parameter. In addition, Kerrigan and Pandis (2017) suggested that the hygroscopicity
503 could exhibit a maximum at intermediate volatilities.

504

505 9. Conclusions

506 The volatility distribution of the OA factors found during the SOAS campaign
507 was estimated using measurements by a thermodenuder coupled with a HR-AMS. Using
508 both the ambient and the thermodenuder data the same four sources were identified
509 compared to the ambient only PMF analysis. The four sources were attributed to MO-
510 OOA, LO-OOA, Isoprene-OA and BBOA. The contribution, the times series and the
511 mass spectra of each factor were similar to the case of the ambient-only PMF. Using the
512 MFRs and the thermodenuder model of Riipinen et al. (2010) the volatility distribution
513 and the vaporization enthalpy of each factor was estimated assuming an accommodation
514 coefficient of unity.

515 MO-OOA was significantly more oxygenated than LO-OOA, but in contrast with
516 previous studies, its MFR was much lower. According to the model, the MO-OOA was
517 less volatile than the LO-OOA and the implausible behavior of the measured MFR was
518 due to their different effective enthalpies of evaporation: 89 ± 10 kJ mol⁻¹ for the MO-



519 OOA and 58 ± 13 kJ mol⁻¹ for the LO-OOA. Isoprene-OA had a similar volatility
520 distribution with MO-OOA, but its vaporization enthalpy was lower at 63 ± 15 kJ mol⁻¹.
521 BBOA had the lowest O:C ratio but it was the least volatile OA component with a
522 vaporization enthalpy of 55 ± 11 kJ mol⁻¹. All factors, included components with a wide
523 range of volatilities, both semi-volatile and low volatility. The use of a relatively modest
524 highest temperature (100°C) did not allow the characterization of the least volatile
525 components of the various factors. The above results suggest that variations in the
526 enthalpy of vaporization can introduce significant variability in the links between the
527 measured MFR and the estimated volatility.

528 The contradicting result of the higher MFR of the MO-OOA compared to that of
529 LO-OOA denotes that depending on the study the behavior of the OOA factors can be
530 quite variable. It shows that OOA factors are composed of organic compounds with a
531 wide range of volatility distributions, which may overlap a lot each other. One possible
532 reason could be the existence of small highly oxygenated molecules. The direct
533 comparison of the MFR of OOA factors from different or even from the same study is
534 risky since MFR depends on the TD operation and characteristics, the aerosol size
535 distribution, the volatility, etc.

536 The counterintuitive finding of Cerully et al. (2015), that Isoprene-OA was more
537 hygroscopic than MO-OOA even though it had a lower O:C ratio, but similar volatility
538 distribution, are close but not fully explained by the framework proposed by Nakao
539 (2017). Future studies are necessary for a comprehensive understanding of the
540 relationship between the hygroscopicity, volatility and O:C ratio.

541

542 **Acknowledgments**

543 This work was funded by the National Oceanic and Atmospheric Administration CPO
544 Award NA10OAR4310102 and the US Environmental Protection Agency (EPA-STAR)
545 through grants RD-835410 and RD-835405. This research was also supported by the
546 European Research Council Project PyroTRACH (Pyrogenic TRansformations Affecting
547 Climate and Health) Grant Agreement 726165. AN, LX, HG, RW and NLN acknowledge
548 support from an NSF grant (1242258). LX and NLN acknowledge support from EPA
549 STAR grant RD-83540301. The contents of this publication are solely the responsibility



550 of the authors and do not necessarily represent the official views of the US EPA. Further,
551 the US EPA does not endorse the purchase of any commercial products or services
552 mentioned in the publication.

553

554

555 **References**

556 Aiken, A. C. et al.: O/C and OM/OC ratios of primary, secondary, and ambient organic
557 aerosols with High Resolution Time-of-Flight Aerosol Mass Spectrometry,
558 Environ. Sci. Technol., 42, 4478–4485, 2008.

559 Aiken, A. C. et al.: Mexico City aerosol analysis during MILAGRO using high resolution
560 aerosol mass spectrometry at the urban supersite (T0) – Part 1: Fine particle
561 composition and organic source apportionment, Atmos. Chem. Phys., 9, 6633–
562 6653, 2009.

563 An, W. J., Pathak, R. K., Lee, B. H., and Pandis, S. N.: Aerosol volatility measurement
564 using an improved thermodenuder: Application to secondary organic aerosol, J.
565 Aerosol Sci., 38, 305–314, 2007.

566 Asa-Awuku, A., Engelhart, G. J., Lee, B. H., Pandis, S. N., and Nenes, A.: Relating CCN
567 activity, volatility, and droplet growth kinetics of β -caryophyllene secondary
568 organic aerosol, Atmos. Chem. Phys., 9, 795–812, 2009.

569 Bretti, C., Crea, F., Foti, C., and Sammartano, S.: Solubility and activity coefficients of
570 acidic and basic nonelectrolytes in aqueous salt solutions. 2. Solubility and
571 activity coefficients of suberic, azelaic, and sebacic acids in NaCl(aq),
572 (CH₃)₄NCl(aq), and (C₂H₅)₄NI(aq) at different ionic strengths and at $t = 25\text{ }^{\circ}\text{C}$, J.
573 Chem. Eng. Data., 51: 1660–1667, 2006.

574 Budisulistiorini, S. H., Nenes, A., Carlton, A. G., Surratt, J. D., McNeill, V. F., Pye, H. O.
575 T.: Simulating aqueous-phase Isoprene-Epoxydiol (IEPOX) secondary organic
576 aerosol production during the 2013 Southern Oxidant and Aerosol Study (SOAS),
577 Environ. Sci. Technol., 51, 5026–5034, 2017.

578 Burtscher, H., Baltensperger, U., Bukowiecki, N., Cohn, P., Hüglin, C., Mohr, M., Matter,
579 U., Nyeki, S., Schmatloch, V., Streit, N., and Weingartner, E.: Separation of



- 580 volatile and non-volatile aerosol fractions by thermodesorption: Instrumental
581 development and applications, *J. Aerosol Sci.*, 32, 427–442, 2001.
- 582 Canagaratna, M. R., Jimenez, J. L., Kroll, J. H., Chen, Q., Kessler, S. H., Massoli, P.,
583 Hildebrandt Ruiz, L., Fortner, E., Williams, L. R., Wilson, K. R., Surratt, J. D.,
584 Donahue, N. M., Jayne, J. T., and Worsnop, D. R.: Elemental ratio measurements
585 of organic compounds using aerosol mass spectrometry: characterization,
586 improved calibration, and implications, *Atmos. Chem. Phys.*, 15, 253–272, 2015.
- 587 Cappa, C. D. and Jimenez, J. L.: Quantitative estimates of the volatility of ambient
588 organic aerosol, *Atmos. Chem. Phys.*, 10, 5409–5424, 2010.
- 589 Carlton, A.G. et al.: The Southeast Atmosphere Studies (SAS): Coordinated investigation
590 and discovery to answer critical questions about fundamental atmospheric
591 processes, *Bul.Am.Met.Soc.*, in review, 2017.
- 592 Cain, K. P. and Pandis, S. N.: A technique for the measurement of organic aerosol
593 hygroscopicity, oxidation level, and volatility distributions, *Atmos. Meas. Tech.*
594 *Discuss.*, amt-2017-213, in review, 2017.
- 595 Cerully, K. M., Hite, J., McLaughlin, M., and Nenes, A.: Towards the determination of
596 joint volatility-hygroscopicity distributions: instrument development and response
597 characterization for single-component aerosol, *Aerosol. Sci. Tech.*, 48, 296–312,
598 2014.
- 599 Cerully, K. M., Bougiatioti, A., Hite Jr., J. R., Guo, H., Xu, L., Ng, N. L., Weber, R., and
600 Nenes, A.: On the link between hygroscopicity, volatility, and oxidation state of
601 ambient and water-soluble aerosols in the southeastern United States, *Atmos.*
602 *Chem. Phys.*, 15, 8679–8694, 2015.
- 603 Chang, R. Y.-W., Slowik, J. G., Shantz, N. C., Vlasenko, A., Liggio, J., Sjostedt, S. J.,
604 Leaitch, W. R., and Abbatt, J. P. D.: The hygroscopicity parameter (κ) of ambient
605 organic aerosol at a field site subject to biogenic and anthropogenic influences:
606 relationship to degree of aerosol oxidation, *Atmos. Chem. Phys.*, 10, 5047–5064,
607 2010.
- 608 Chen, N. H., and Othmer, D. F.: New generalized equation for gas diffusion coefficient, *J.*
609 *Chem. Eng. Data*, 7, 37–41, 1962.



- 610 Cohen A. J. et al.: Estimates and 25-year trends of the global burden of disease
611 attributable to ambient air pollution: an analysis of data from the Global Burden
612 of Diseases Study 2015, *The Lancet*, 389, 10082, 1907–1918, 2017.
- 613 Crippa, M., et al.: Wintertime aerosol chemical composition and source apportionment of
614 the organic fraction in the metropolitan area of Paris, *Atmos. Chem. Phys.*, 13,
615 961–981, 2013.
- 616 DeCarlo, P.F., Kimmel, J. R., Trimborn, A., Northway, M. J., Jayne, J. T., Aiken, A. C.,
617 Gonin, M., Fuhrer, K., Horvath, T., Docherty, K., Worsnop, D. R., and Jimenez, J.
618 L.: Field-Deployable, High-Resolution, Time-of-Flight Aerosol Mass
619 Spectrometer, *Analytical Chemistry*, 78: 8281-8289, 2006.
- 620 Donahue, N. M., Kroll, J. H., Pandis, S. N., and Robinson, A. L.: A two-dimensional
621 volatility basis set – Part 2: Diagnostics of organic-aerosol evolution, *Atmos.*
622 *Chem. Phys.*, 12, 615–634, 2012.
- 623 Faulhaber, A. E., Thomas, B. M., Jimenez, J. L., Jayne, J. T., Worsnop, D. R., and
624 Ziemann, P. J.: Characterization of a thermodenuder-particle beam mass
625 spectrometer system for the study of organic aerosol volatility and composition,
626 *Atmos. Meas. Tech.*, 2, 15-31, 2009.
- 627 Florou, K., Papanastasiou, D. K., Pikridas, M., Kaltsonoudis, C., Louvaris, E., Gkatzelis,
628 E., Patoulias, D., Mihalopoulos, N., and Pandis, S. N.: The contribution of wood
629 burning and other pollution sources to wintertime organic aerosol levels in two
630 Greek cities, *Atmos. Chem. Phys.*, 17, 3145-3163, 2017.
- 631 Frosch, M., Bilde, M., Nenes, A., Praplan, A. P., Jurányi, Z., Dommen, J., Gysel, M.,
632 Weingartner, E., and Baltensperger, U.: CCN activity and volatility of β -
633 caryophyllene secondary organic aerosol, *Atmos. Chem. Phys.*, 13, 2283–2297,
634 2013.
- 635 Fuchs, N.A., and Sutugin, A.G.: Highly Dispersed Aerosols. Ann Arbor Science
636 Publishers, Ann Arbor, London, 1970.
- 637 Guo, H., Xu, L., Bougiatioti, A., Cerully, K. M., Capps, S. L., Hite Jr., J. R., Carlton, A.
638 G., Lee, S.-H., Bergin, M. H., Ng, N. L., Nenes, A., and Weber, R. J.: Fine-
639 particle water and pH in the southeastern United States, *Atmos. Chem. Phys.*, 15,
640 5211-5228, 2015.



- 641 Hallquist, M. J. C. et al.: The formation, properties and impact of secondary organic
642 aerosol: current and emerging issues, *Atmos. Chem. Phys.*, 9, 5155-5236, 2009.
- 643 Hu, W. et al.: Characterization of a real-time tracer for isoprene epoxydiols-derived
644 secondary organic aerosol (IEPOX-SOA) from aerosol mass spectrometer
645 measurements, *Atmos. Chem. Phys.*, 15, 11807-11833, 2015.
- 646 Hu, W. et al.: Volatility and lifetime against OH heterogeneous reaction of ambient
647 isoprene-epoxydiols-derived secondary organic aerosol (IEPOX-SOA), *Atmos.*
648 *Chem. Phys.*, 16, 11563-11580, 2016.
- 649 Huffman, J. A., Docherty, K. S., Aiken, A. C., Cubison, M. J., Ulbrich, I. M., DeCarlo, P.
650 F., Sueper, D., Jayne, J. T., Worsnop, D. R., Ziemann, P. J., and Jimenez, J. L.:
651 Chemically-resolved aerosol volatility measurements from two megacity field
652 studies, *Atmos. Chem. Phys.*, 9, 7161–7182, 2009.
- 653 Jimenez, J. L. et al.: Evolution of organic aerosols in the atmosphere, *Science*, 326,
654 1525–1529, 2009.
- 655 IARC (International Agency for Research on Cancer). In press. Outdoor Air Pollution.
656 IARC Monogr. Eval. Carcinog. Risks Hum 109.
- 657 IPCC, Intergovernmental Panel on Climate Change, *Climate change 2013: The Physical*
658 *Science Basis*. Cambridge University Press, Cambridge, 2013.
- 659 Kanakidou, M. et al.: Organic aerosol and global climate modelling: a review, *Atmos.*
660 *Chem. Phys.*, 5, 1053-1123, 2005.
- 661 Karnezi, E., Riipinen, I., and Pandis, S. N.: Measuring the atmospheric organic aerosol
662 volatility distribution: a theoretical analysis, *Atmos. Meas. Tech.*, 7, 2953–2965,
663 2014.
- 664 Kostenidou, E., Florou, K., Kaltsonoudis, C., Tsiglikiotou, M., Vratolis, S., Eleftheriadis,
665 K., and Pandis, S. N.: Sources and chemical characterization of organic aerosol
666 during the summer in the eastern Mediterranean, *Atmos. Chem. Phys.*, 15, 11355-
667 11371, 2015.
- 668 Kostenidou, E., Karnezi, E., Kolodziejczyk, A., Szmigielski, R., and Pandis, S. N.:
669 Physical and chemical properties of 3-methyl-1,2,3-butanetricarboxylic acid
670 (MBTCA) aerosol, *Environ. Sci. Technol.*, submitted, 2017.



- 671 Kuwata, M., Kondo, Y., Mochida, M., Takegawa, N., and Kawamura, K.: Dependence of
672 CCN activity of less volatile particles on the amount of coating observed in
673 Tokyo, *J. Geophys. Res.*, 112, D11207, doi:10.1029/2006JD007758, 2007.
- 674 Lanz, V. A., Alfarra, M. R., Baltensperger, U., Buchmann, B., Hueglin, C., and Prévôt, A.
675 S. H.: Source apportionment of submicron organic aerosols at an urban site by
676 factor analytical modeling of aerosol mass spectra, *Atmos. Chem. Phys.*, 7, 1503–
677 1522, 2007.
- 678 Lanz, V. A., Alfarra, M. R., Baltensperger, U., Buchmann, B., Hueglin, C., Szidat, S.,
679 Wehrl, M. N., Wacker, L., Weimer, S., Caseiro, A., Puxbaum, J., and Prévôt, A.
680 S. H.: Source attribution of submicron organic aerosols during wintertime
681 inversions by advanced factor analysis of aerosol mass spectra, *Environ. Sci.*
682 *Technol.*, 42, 214-220, 2008.
- 683 Latham, T. L., Beyersdorf, A. J., Thornhill, K. L., Winstead, E. L., Cubison, M. J.,
684 Hecobian, A., Jimenez, J. L., Weber, R. J., Anderson, B. E., and Nenes, A.:
685 Analysis of CCN activity of Arctic aerosol and Canadian biomass burning during
686 summer 2008, *Atmos. Chem. Phys.*, 13, 2735–2756, 2013.
- 687 Lee, B. H., Kostenidou, E., Hildebrandt, L., Riipinen, I., Engelhart, G. J., Mohr, C.,
688 DeCarlo, P. F., Mihalopoulos, N., Prevot, A. S. H., Baltensperger, U., and Pandis,
689 S. N.: Measurement of the ambient organic aerosol volatility distribution:
690 application during the Finokalia Aerosol Measurement Experiment (FAME-
691 2008). *Atmos. Chem. Phys.*, 10, 12149-12160, 2010.
- 692 Lee, B. H., Pierce, J. R., Engelhart, G. J., and Pandis, S. N.: Volatility of secondary
693 organic aerosol from the ozonolysis of monoterpenes. *Atmos. Environ.*, 45, 2443-
694 2452, 2011.
- 695 Liao, H., Henze, D. K., Seinfeld, J. H., Wu, S., and Mickley, L. J.: Biogenic secondary
696 organic aerosol over the United States: Comparison of climatological simulations
697 with observations, *J. Geophys. Res.*, 112, D06201, doi:10.1029/2006JD007813,
698 2007.
- 699 Lopez-Hilfiker, F. D., Mohr, C., D'Ambro, E. L., Lutz, A., Riedel, T. P., Gaston, C. J.,
700 Iyer, S., Zhang, X., Gold, A., Surratt, J. D., Lee, B. H., Kurten, T., Hu, W. W.,
701 Jimenez, J., Hallquist, M., and Thornton, J. A.: Molecular composition and



- 702 volatility of organic aerosol in the Southeastern U.S.: Implications for IEPOX
703 derived SOA. *Environ. Sci. Technol.*, 50, (5), 2200-2209, 2016.
- 704 Louvaris, E., Florou, K., Karnezi, E., Papanastasiou, D. K., Gkatzelis, G. I., and Pandis, S.
705 N.: Volatility of source apportioned wintertime organic aerosol in the city of
706 Athens, *Atmos. Environ.*, 158, 138-147, 2017.
- 707 Meyer, N. K., Duplissy, J., Gysel, M., Metzger, A., Dommen, J., Weingartner, E., Alfarra,
708 M. R., Prevot, A. S. H., Fletcher, C., Good, N., McFiggans, G., Jonsson, Å. M.,
709 Hallquist, M., Baltensperger, U., and Ristovski, Z. D.: Analysis of the
710 hygroscopic and volatile properties of ammonium sulphate seeded and unseeded
711 SOA particles, *Atmos. Chem. Phys.*, 9, 721–732, 2009.
- 712 Middlebrook, A. M., Bahreini, R., Jimenez, J.L., and Canagaratna, M. R.: Evaluation of
713 composition - dependent collection efficiencies for the Aerodyne Aerosol Mass
714 Spectrometer using field data, *Aerosol Sci. Tech.*, 46, 258 - 271, 2012.
- 715 Moore, R. H. and Nenes, A.: Scanning flow CCN analysis – a method for fast
716 measurements of CCN spectra, *Aerosol Sci. Tech.*, 43, 1192–1207, 2009.
- 717 Nakao, S.: Why would apparent κ linearly change with O/C? Assessing the Role of
718 Volatility, Solubility, and Surface Activity of Organic Aerosols, *Aerosol Sci.*
719 *Tech.*, under revision, 2017.
- 720 National Academies of Sciences, Engineering, and Medicine: The Future of Atmospheric
721 Chemistry Research: Remembering Yesterday, Understanding Today,
722 Anticipating Tomorrow Washington, DC, The National Academies Press. doi:
723 10.17226/235730, 2016.
- 724 Ng, N. L. et al.: Organic aerosol components observed in Northern Hemispheric datasets
725 from Aerosol Mass Spectrometry, *Atmos. Chem. Phys.*, 10, 4625– 4641, 2010.
- 726 Ortiz-Montalvo, D. L., Lim, Y. B., Perri, M. P., Seitzinger, S. P., and Turpin, B. J.:
727 Volatility and yield of glycolaldehyde SOA formed through aqueous
728 photochemistry and droplet evaporation, *Aerosol Sci. Tech.*, 46, 1002–1014, 2012.
- 729 Paatero, P. and Tapper, U.: Positive matrix factorization – a nonnegative factor model
730 with optimal utilization of error-estimates of data values, *Environmetrics*, 5, 111–
731 126, 1994.



- 732 Paciga, A., Karnezi, E., Kostenidou, E., Hildebrandt, L., Psichoudaki, M., Engelhart, G.
733 J., Lee, B.-H., Crippa, M., Prévôt, A. S. H., Baltensperger, U., and Pandis, S. N.:
734 Volatility of organic aerosol and its components in the megacity of Paris, Atmos.
735 Chem. Phys., 16, 2013–2023, 2016.
- 736 Peng, C., Chan, M. N., and Chan, C. K.: The hygroscopic properties of dicarboxylic and
737 multifunctional acids: measurements and UNIFAC predictions, Environ. Sci.
738 Technol., 35, 4495–4501, 2001.
- 739 Pope, C. A., Burnett, R. T., Thun, M. J., Calle, E. E., Krewski, D., Ito, K., Thurston, G.
740 D.: Lung cancer, cardiopulmonary mortality, and long-term exposure to fine
741 particulate air pollution, JAMA, 287, 1132–41, 2002.
- 742 Rastak, N., A. et al.: Microphysical explanation of the RH-dependent water-affinity of
743 biogenic organic aerosol and its importance for climate, Geoph. Res. Let., 44,
744 doi:10.1002/2017GL073056, 2017.
- 745 Riipinen, I., Pierce, J. R., Donahue, N. M., and Pandis, S. N.: Equilibration time scales of
746 organic aerosol inside thermodenuders: Evaporation kinetics versus
747 thermodynamics, Atmos. Environ., 44, 597–607, 2010.
- 748 Roberts, G. C., and Nenes, A.: A continuous-flow streamwise thermal-gradient CCN
749 chamber for atmospheric measurements, Aerosol Sci. Tech., 39, 206–221, 2005.
- 750 Saha, P. K., and Grieshop, A. P.: Exploring divergent volatility properties from yield and
751 thermodenuder measurements of secondary organic aerosol from α -pinene
752 ozonolysis, Environ. Sci. Technol., 50, 5740–5749, 2016.
- 753 Saha, P. K., Khlystov, A., Yahya, K., Zhang, Y., Xu, L., Ng, N. L., and Grieshop, A. P.:
754 Quantifying the volatility of organic aerosol in the southeastern US, Atmos. Chem.
755 Phys., 17, 501–520, 2017.
- 756 Saleh, R., Walkerb, J., and Khlystov, A.: Determination of saturation pressure and
757 enthalpy of vaporization of semi-volatile aerosols: The integrated volume method,
758 Aerosol Science, 39, 876–887, 2008.
- 759 Saleh, R., Khlystov, A., and Shihadeh, A.: Effect of aerosol generation method on
760 measured saturation pressure and enthalpy of vaporization for dicarboxylic acids
761 aerosol, Aerosol Sci. Tech., 44, 302–307, 2010.



- 762 Saleh, R., Shihadeh, A., and Khlystov, A.: On transport phenomena and equilibration
763 time scales in thermodenuders, *Atmos. Meas. Tech.*, 4, 571–581, 2011.
- 764 Saxena, P., and Hildemann, L.: Water-soluble organics in atmospheric particles: a critical
765 view of the literature and application of thermodynamics to identify candidate
766 compounds. *J. Atmos. Chem.*, 24, 57-109, 1996.
- 767 Seinfeld, J. H. et al.: Improving our fundamental understanding of the role of aerosol-
768 cloud interactions in the climate system, *P. Natl. Acad. Sci.*, 113, 21, 5781-5790,
769 2016.
- 770 Spracklen, D. V., Jimenez, J. L., Carslaw, K. S., Worsnop, D. R., Evans, M. J., Mann, G.
771 W., Zhang, Q., Canagaratna, M. R., Allan, J., Coe, H., McFiggans, G., Rap, A.,
772 and Forster, P.: Aerosol mass spectrometer constraint on the global secondary
773 organic aerosol budget, *Atmos. Chem. Phys.*, 11, 12109-12136, 2011.
- 774 Stephenson, R. M. and Malanowski, S.: *Handbook of the Thermodynamics of Organic*
775 *Compounds*, 1987.
- 776 Thalman, R. et al.: CCN activity and organic hygroscopicity of aerosols downwind of an
777 urban region in central Amazonia: Seasonal and diel variations and impact of
778 anthropogenic emissions, *Atmos. Chem. Phys. Discuss.*,
779 <https://doi.org/10.5194/acp-2017-251>, in review, 2017.
- 780 Tritscher, T., Dommen, J., DeCarlo, P. F., Gysel, M., Barmet, P. B., Praplan, A. P.,
781 Weingartner, E., Prévôt, A. S. H., Riipinen, I., Donahue, N. M., and Baltensperger,
782 U.: Volatility and hygroscopicity of aging secondary organic aerosol in a smog
783 chamber, *Atmos. Chem. Phys.*, 11, 11477–11496, 2011.
- 784 Ulbrich, I. M., Canagaratna, M. R., Zhang, Q., Worsnop, D. R., and Jimenez, J. L.:
785 Interpretation of organic components from Positive Matrix Factorization of
786 aerosol mass spectrometric data, *Atmos. Chem. Phys.*, 9, 2891–2918, 2009.
- 787 Vesala, T., Kulmala, M., Rudolf, R., Vrtala, A., and Wagner, P. E.: Models for
788 condensational growth and evaporation of binary aerosol particles, *J. Aerosol Sci.*
789 28, 565-598, 1997.
- 790 Weber, R. J., Orsini, D., Daun, Y., Lee, Y.-N., Klotz, P., and Brechtel, F.: A particle-into-
791 liquid collector for rapid measurements of aerosol chemical composition, *Aerosol*
792 *Sci. Tech.*, 35, 718–727, 2001.



- 793 Xu, L., Guo, H., Boyd, C. M., Klein, M., Bougiatioti, A., Cerully, K. M., Hite, J. R.,
794 Isaacman-VanWertz, G., Kreisberg, N. M., Knote, C., Olson, K., Koss, A.,
795 Goldstein, A. H., Hering, S. V., de Gouw, J., Baumann, K., Lee, S-H., Nenes, A.,
796 Weber, R. J., and Ng, N. L.: Effects of anthropogenic emissions on aerosol
797 formation from isoprene and monoterpenes in the Southeastern United States, P.
798 Natl. Acad. Sci., 112, 37–42, 2015a.
- 799 Xu, L., Suresh, S., Guo, H., Weber, R. J., and Ng, N. L.: Aerosol characterization over
800 the southeastern United States using High-Resolution Aerosol Mass
801 Spectrometry: spatial and seasonal variation of aerosol composition and sources
802 with a focus on organic nitrates, Atmos. Chem. Phys., 15, 7307-7336, 2015b.
- 803 Xu, L., et al.: Enhanced formation of isoprene-derived organic aerosol in power plant
804 plumes during Southeast Nexus (SENEX), J. Geoph. Res., 121, doi:
805 10.1002/2016JD025156, 2016a.
- 806 Xu, L., Williams, L. R., Young, D. E., Allan, J. D., Coe, H., Massoli, P., Fortner, E.,
807 Chhabra, P., Herndon, S., Brooks, W. A., Jayne, J. T., Worsnop, D. R., Aiken, A.
808 C., Liu, S., Gorkowski, K., Dubey, M. K., Fleming, Z. L., Visser, S., Prévôt, A. S.
809 H., and Ng, N. L.: Wintertime aerosol chemical composition, volatility, and
810 spatial variability in the greater London area, Atmos. Chem. Phys., 16, 1139-1160,
811 2016b.
- 812 Xu, L., Guo, H., Weber, R. J., and Ng, N. L.: Chemical characterization of water soluble
813 soluble organic aerosol in contrasting rural and urban environments in the
814 Southeastern United States, Environ. Sci. Technol., 51, 78-88, 2017.
- 815 Zhang, Q., Alfarra, M. R., Worsnop, D. R., Allan, J. D., Coe, H., Canagaratna, M., and
816 Jimenez, J. L.: Deconvolution and quantification of hydrocarbon-like and
817 oxygenated organic aerosols based on aerosol mass spectrometry, Environ. Sci.
818 Technol., 39, 4938-4952, 2005.
- 819 Zhang, Q. et al.: Ubiquity and dominance of oxygenated species in organic aerosols in
820 anthropogenically-influenced Northern Hemisphere midlatitudes, Geophys. Res.
821 Lett., 34, L13801, doi: 10.1029/2007gl029979, 2007.
- 822



823

824

825

826 **Table 1.** Average ambient concentration of each factor and total OA, and the
827 corresponding fraction of the data above the threshold ($0.2 \mu\text{g m}^{-3}$).

828

Factor	Average Ambient Concentration ($\mu\text{g m}^{-3}$)	% of Measurements above the Threshold
MO-OOA	1.96	92
LO-OOA	1.66	96
Isoprene-OA	0.9	76
BBOA	0.5	42
Total OA	5.02	99

829

830

831

832

833

834

835

836

837

838

839

840

841

842

843

844

845

846

847

848

849

850

851

852

853

854

855

856



857
858
859
860
861
862
863
864
865

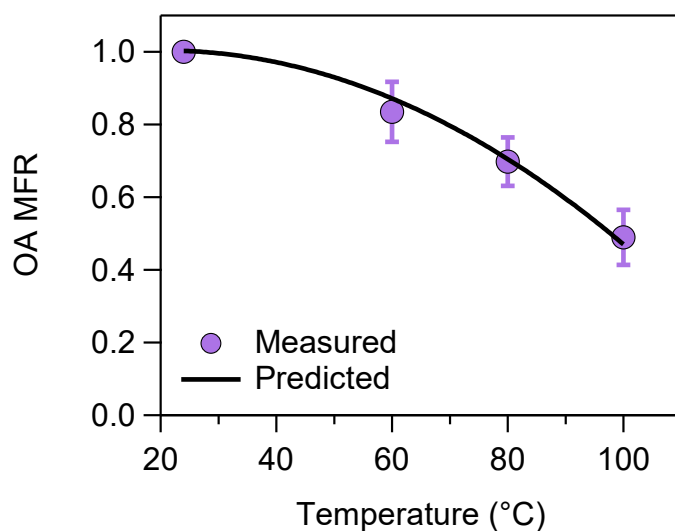
Table 2. OA mass fractions of the ambient and ambient+TD PMF factors.

Data Used	MO-OOA (%)	LO-OOA (%)	Isoprene-OA (%)	BBOA (%)
Ambient only	39	32	18	10
Ambient+TD	43	29	19	9

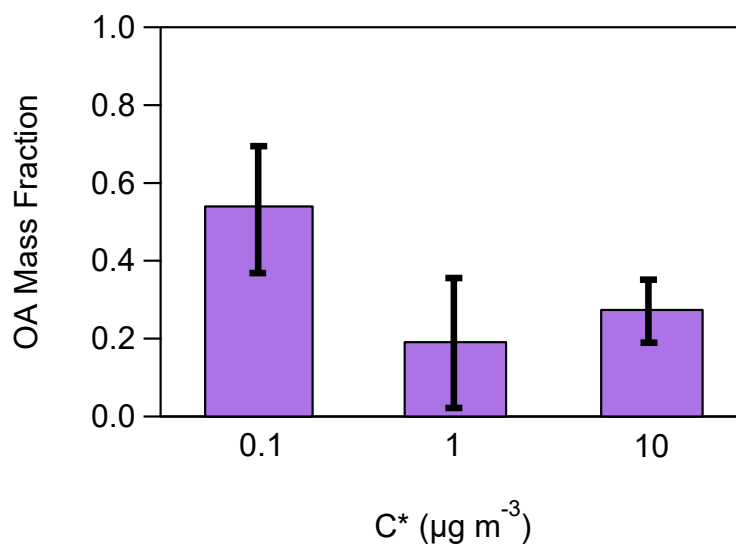
866
867
868
869
870
871
872
873
874
875
876
877
878
879
880
881
882
883
884
885
886
887
888
889
890
891
892
893
894
895
896
897



898
899
900
901
902



903

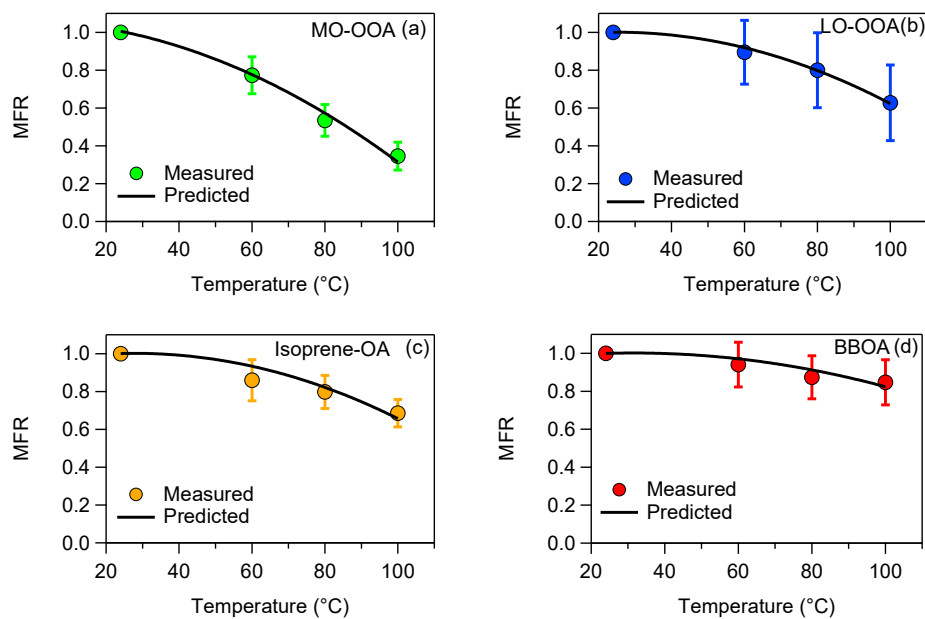


904
905

906 **Figure 1.** (a) Loss-corrected MFR of the total OA. The purple circles correspond to the
907 measurements and the uncertainties to one standard deviation of the mean. It is assumed
908 that MFR=1 at T=24°C. The black line is the model fit estimated using the approach of



909 Karnezi et al. (2014). (b) The total OA volatility distribution. The uncertainties have been
910 estimated according to the algorithm of Karnezi et al. (2014).
911



912

913

914

915 **Figure 2.** MFRs of the loss-corrected PMF OA factors. The circles represent the
916 measurements with the one standard deviation of the mean. The black line corresponds to
917 the best predicted MFR using the algorithm of Karnezi et al. (2014).

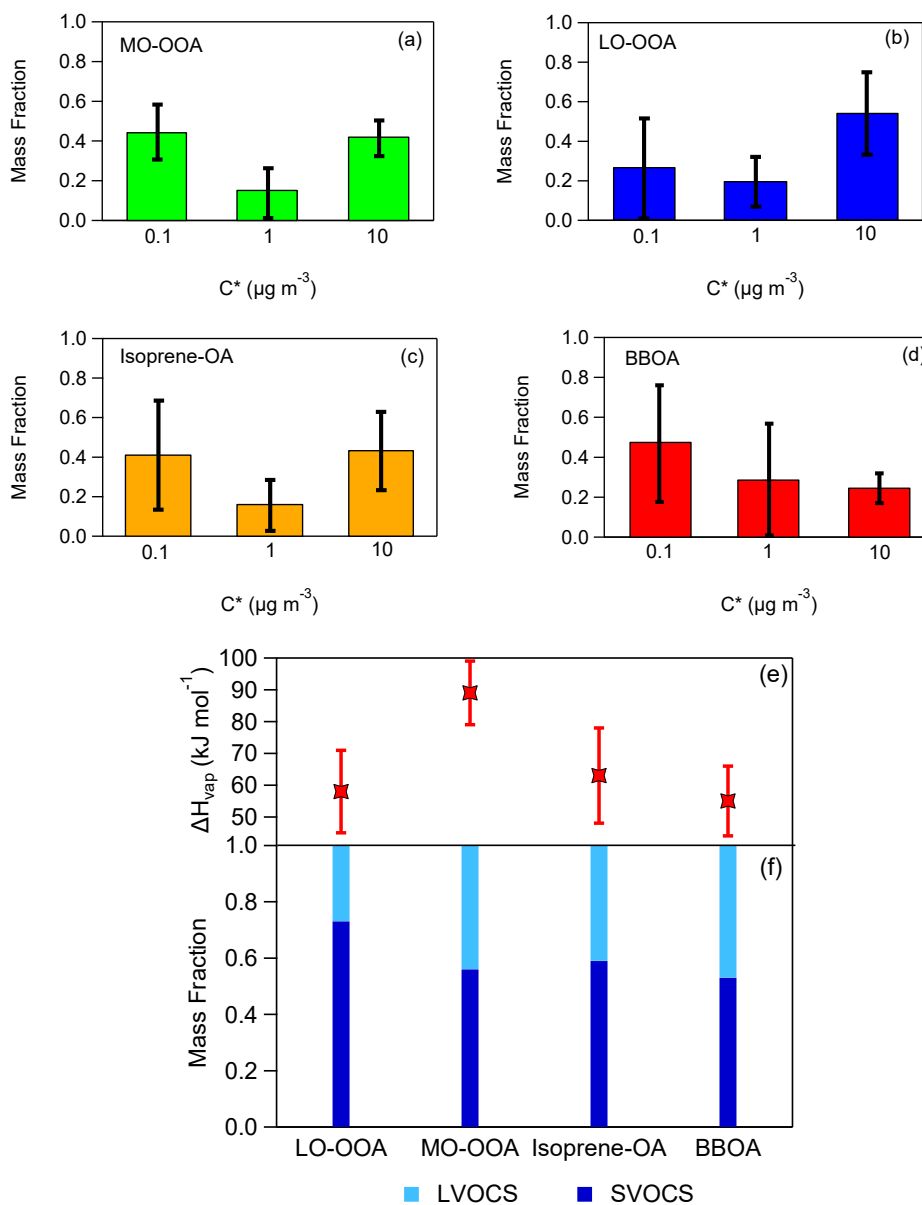
918

919

920

921

922



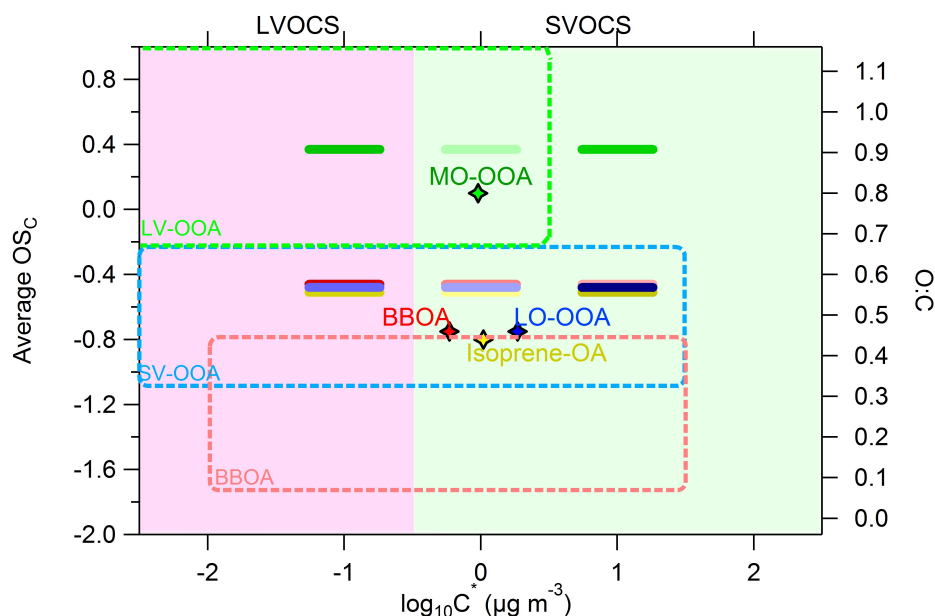
923

924

925

926

927 **Figure 3.** (a)-(d) Predicted volatility distributions of the OA PMF factors. The error bars
 928 correspond to the uncertainties derived using the approach of Karnezi et al. (2014), (e)
 929 vaporization enthalpies comparison between the four OA factors and (f) volatility
 930 compositions comparison between the four OA factors.



931

932

933 **Figure 4.** Average carbon oxidation state OS_C (left y axis) and O:C ratio (right axis)
934 versus the saturation concentration in terms of $\log_{10}C^*$. The horizontal bars are the
935 volatility distributions of the SOAS PMF factors: MO-OOA (green), LO-OOA (blue),
936 Isoprene-OA (yellow) and BBOA (red). The darker the color of the horizontal bars the
937 higher the mass fractional contribution for the corresponding C^* bin. The diamonds
938 represent the average $\log_{10}C^*$ value for a given PMF factor. The green, light blue and
939 pink dashed areas are the locations of the LV-OOA, SV-OOA and BBOA PMF factors as
940 proposed by Donahue et al. (2012).

941

942

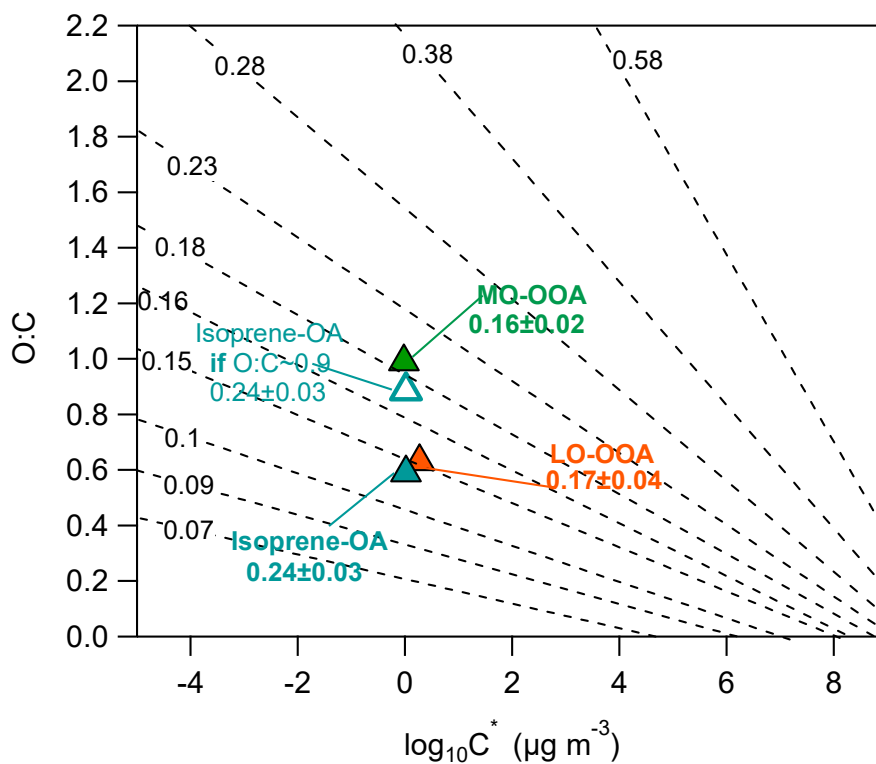
943

944

945

946

947



948

949

950 **Figure 5.** O:C ratios versus the average volatility as $\log_{10}C^*$. The black isolines951 correspond to the theoretically intrinsic κ suggested by Nakao et al. (2017). The triangles

952 denote the SOAS PMF factors. The hygroscopicity of the SOAS PMF factors has been

953 transformed into the intrinsic κ , using the water solubility results of Xu et al. (2017). The

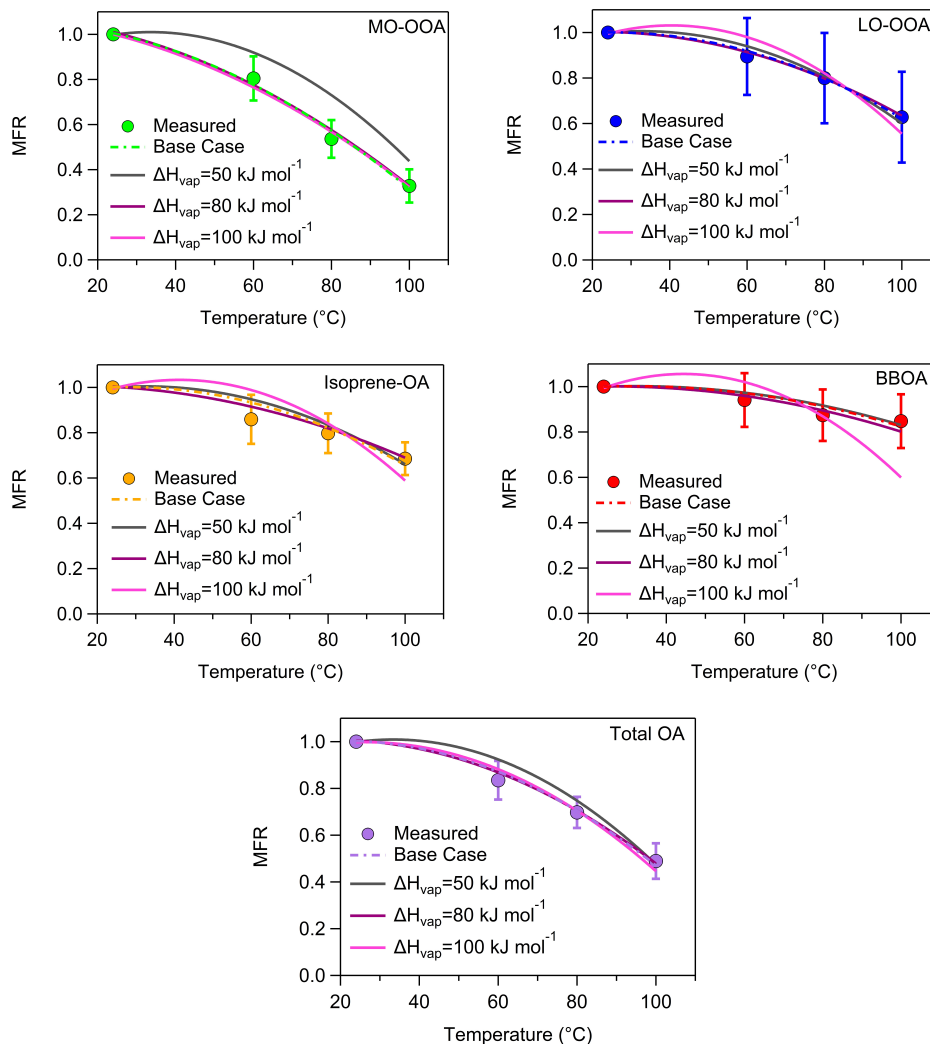
954 open cyan triangle corresponds to the Isoprene-OA with a hypothetical O:C=0.9.

955



956

957 **Appendix**



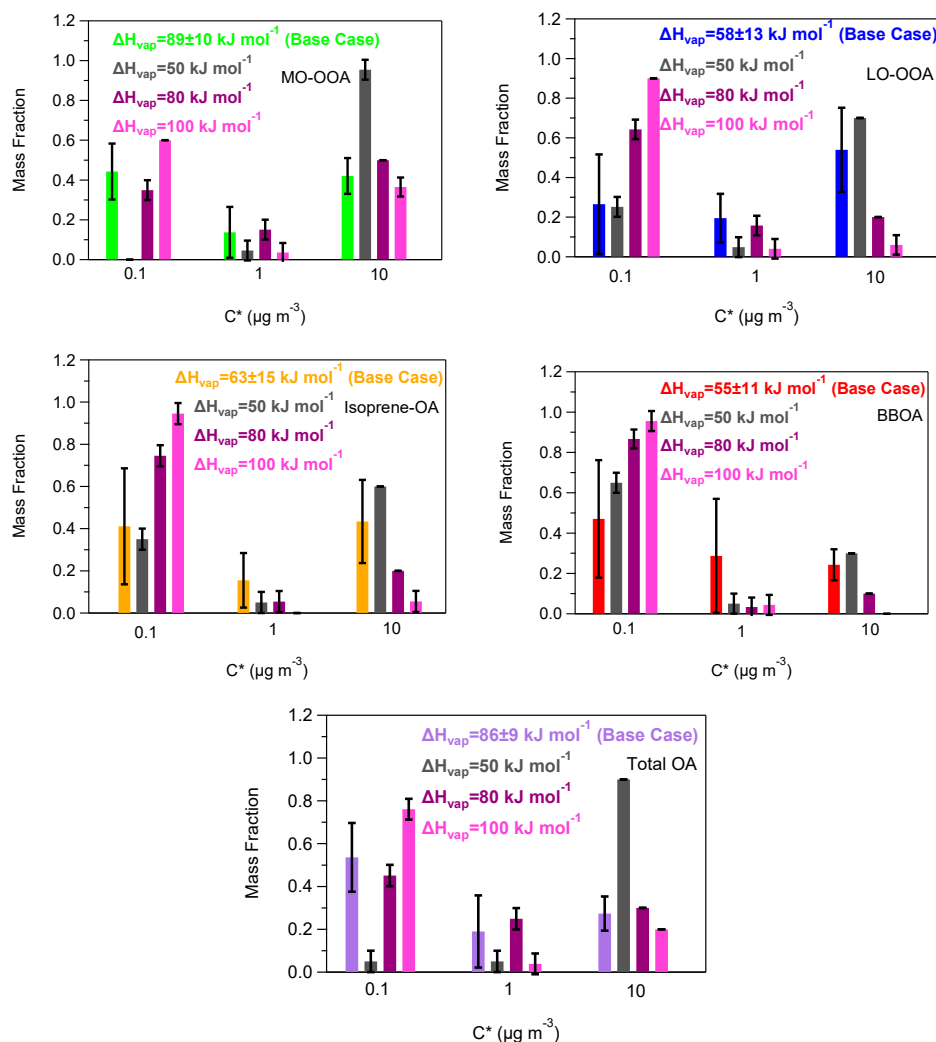
958

959

960

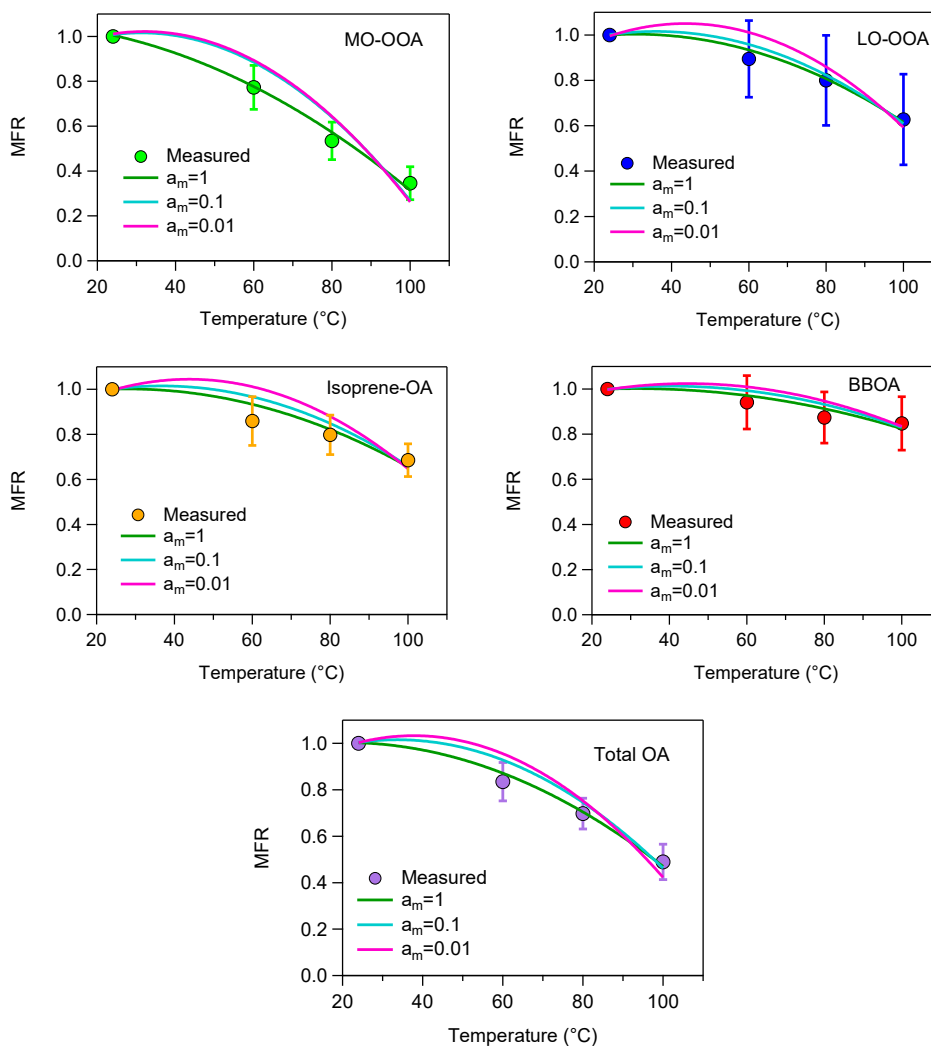
961 **Figure A1.** MFRs of the loss-corrected PMF OA factors and total OA for fixed values of
962 the vaporization enthalpy. The circles denote the measurements with the one standard
963 deviation of the mean, the dash lines correspond to the base case, the grey lines represent
964 the case of a constant ΔH_{vap} of 50 kJ mol⁻¹, the magenta lines stand for the case of a
965 constant ΔH_{vap} of 80 kJ mol⁻¹ and the pink lines correspond to the case of a constant
966 ΔH_{vap} of 100 kJ mol⁻¹.

967



971 **Figure A2.** Predicted volatility distributions of the OA PMF factors and total OA for
 972 fixed vaporization enthalpy. The error bars are estimated using the approach of Karnezi et
 973 al. (2014). The grey bars represent the results of a constant ΔH_{vap} of 50 kJ mol^{-1} , the
 974 magenta bars correspond to the solution of a constant ΔH_{vap} of 80 kJ mol^{-1} , while and the
 975 pink bars are the results for the case of a constant ΔH_{vap} of 100 kJ mol^{-1} . The green, blue,
 976 orange, red and purple bars stand for the base case solutions of MO-OOA, LO-OOA,
 977 Isoprene-OA, BBOA and total OA.

978



983

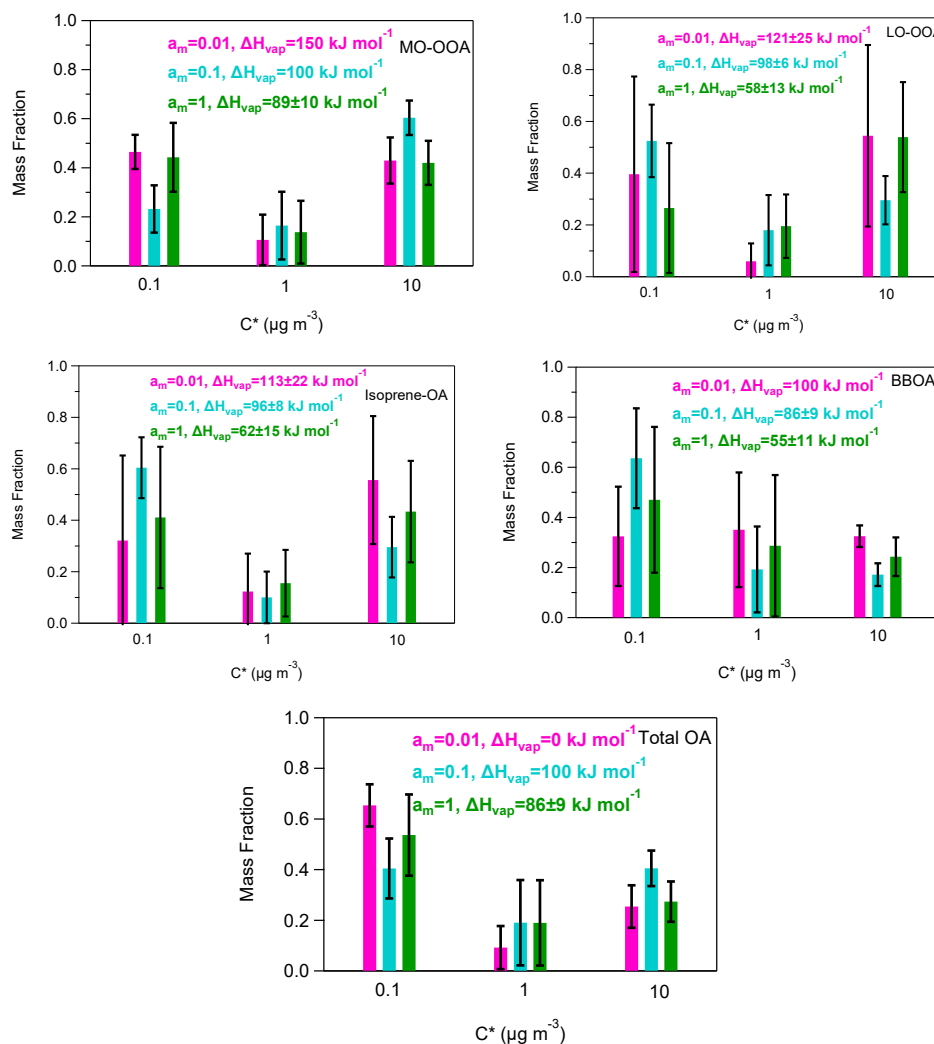
984

985

986

987

Figure A3. MFRs of the loss-corrected PMF OA factors and total OA. The circles denote the measurements with the one standard deviation of the mean, the green lines represent the best predicted MFR for $a_m=1$ (base case), the cyan lines correspond to the best predicted MFR for $a_m=0.1$, while the pink lines stand for the predicted MFR for $a_m=0.01$.



990

991 **Figure A4.** Predicted volatility distributions of the OA PMF factors and total OA. The
 992 error bars are estimated using the approach of Karnezi et al. (2014). The green bars
 993 represent the results for $a_m=1$ (base case), the cyan bars correspond to the solution for
 994 $a_m=0.1$, while and the pink bars are the results for $a_m=0.01$.

995